

RSC Advances



This is an *Accepted Manuscript*, which has been through the Royal Society of Chemistry peer review process and has been accepted for publication.

Accepted Manuscripts are published online shortly after acceptance, before technical editing, formatting and proof reading. Using this free service, authors can make their results available to the community, in citable form, before we publish the edited article. This *Accepted Manuscript* will be replaced by the edited, formatted and paginated article as soon as this is available.

You can find more information about *Accepted Manuscripts* in the [Information for Authors](#).

Please note that technical editing may introduce minor changes to the text and/or graphics, which may alter content. The journal's standard [Terms & Conditions](#) and the [Ethical guidelines](#) still apply. In no event shall the Royal Society of Chemistry be held responsible for any errors or omissions in this *Accepted Manuscript* or any consequences arising from the use of any information it contains.

Borate Ester Endcapped Fluorescent Hyperbranched Conjugated Polymer for Trace Peroxide Explosive Vapor Detection

Cite this: DOI: 10.1039/x0xx00000x

Received 00th January 2012, Accepted 00th January 2012

Lei Chen^{a,b}, Yixun Gao^{a,b}, Yanyan Fu^a, Defeng Zhu^a, Qingguo He^{a*}, Huimin Cao^a and Jianguo Cheng*

DOI: 10.1039/x0xx00000x

www.rsc.org/

Peroxide explosives (PEs) vapor is difficult to be detected by fluorescent probe because PEs are not typical quenching agents without nitro groups or aromatic units, which can easily interact with electron-rich probes. Three borate ester endcapped pyrenyl-fluorene copolymers were reported for PEs detection including a hyperbranched polymer (S1) and two linear polymers with borate ester on fluorenyl (S2) or pyrenyl (S3) units. It shows that the hyperbranched polymer S1 has a larger steric hindrance, more external borate ester groups, higher HOMO level and fluorescent quantum yield, which make it higher sensitivity to H₂O₂ vapor than S2 and S3. To further amplify the sensing performance toward H₂O₂ vapor, a polymer/ZnO nanorod array composite was used utilizing the catalytic ability and high area to volume ratio of ZnO nanorod array. The fluorescence of S1 film is ~ 60% and ~ 30% quenched under saturated vapor of H₂O₂ and TATP respectively for 300 s at room temperature and the detection limit to H₂O₂ is estimated to be 1.6 ppb. These results reveal that S1/ZnO nanorod array composite is very hopeful for preparing a highly sensitive fluorescence device for detecting peroxide explosives vapor detection.

1. Introduction

During the past decade, social instability, terrorist activities and other criminals have made the enormous harm to human health and social stability¹⁻². A major concern in the field of public safety today is to continue to develop high sensitive sensors for a fast and accurate identification of trace explosives³⁻⁷. The technology of fluorescence sensing based on fluorescent organic molecules has been intensively investigated recently because it has the advantages of high sensitivity, good specificity, rapid response, portability and simple operation. Many studies have been carried out on this technology which is widely used in trace detection of ions, biological molecules, explosives and environmental pollutants⁸⁻¹³.

Peroxide-based explosives (PEs) such as triacetone triperoxide (TATP) are increasingly used to making improvised explosive devices in some crime and terrorism activities¹⁴⁻¹⁵ because of their simple preparation from readily available materials¹⁶ (TATP, just three ingredients: hydrogen peroxide (H₂O₂), an acid and acetone), poor chemical stability and easy decomposition leading to large explosive power. Compared to the nitroaromatic explosives, e.g. 2,4,6-trinitrotoluene (TNT), peroxide explosives vapor is difficult to be detected with fluorescence probe because PEs are not typical quenching agents without nitro groups or aromatic units, which can easily interact with electron-rich chromophores by intermolecular π - π stacking interaction. In addition, sensitivity to mechanical stress, low stability, limited solubility and so on also make the detection of PEs become more challenging¹⁷⁻¹⁸. For example, Germain *et al.* introduced a fluorescence detection method targeted H₂O₂ by using a chelator formed *via* reaction with H₂O₂, which was only limited in liquid phase¹⁹. Prof. Deqing Zhang *et al.* and Hong Qun Luo *et al.* have also developed interesting strategies for the detection of hydrogen peroxide and glucose with two different types of fluorescence probes in

liquid solution²⁰⁻²¹, which is especially suitable for a biological detection. But for peroxide explosive detection, the response rate of liquid phase detection is slow (larger than 30 min) possibly due to a slow solute diffusion process and the additives in the probe synthesis may make the detection complicated. Todd *et al.* reported a method using cavity ringdown spectroscopy (CRDS) for the detection of TATP vapor phase but overlapped absorption bands may occur for air samples containing several analytes leading to the limited selectivity²². Moreover, there are some other methods for PEs detection such as gas chromatography/mass spectrometry (GC/MS), selected-ion flow tube mass spectrometry (SIFT-MS) and ion mobility spectrometry (IMS), but they request either complex operation or heavy equipments, which greatly improve the detection cost and reduce the detection efficiency²³⁻²⁵.

Ling Zang *et al.* reported a fluorescence turn-on molecule and a fluorescence ratiometric sensor molecule respectively by a deboration reaction for trace vapor detection of H₂O₂²⁶⁻²⁷. They are all based on small molecules by a fluorescence enhancement or change of emission wavelength and only H₂O₂ were checked. In this contribution, we reported three kinds of borate ester endcapped pyrenyl-fluorene copolymers based on fluorescence "turn-off" for peroxide vapor including H₂O₂ and TATP detection. The polymers were synthesized *via* Suzuki coupling reaction as shown in **Figure 1**, which were a hyperbranched polymer (S1) and two linear polymers with borate ester on fluorenyl (S2) or pyrenyl (S3) units, respectively. For an efficient detection, both molecular structure and morphology of the film are critical. In molecular structure aspect, both pyrene and fluorene derivatives are important building blocks in fluorescent materials for their relatively simple molecular structure, easy modification and high fluorescence quantum efficiency. And borate ester units, as the chain end groups, were introduced to selectively detect

peroxides. In addition, amplified fluorescence signal could improve the sensing properties *via* the “molecular wires” or the hyperbranched conjugated structure of polymers. In particular, properties associated with the hyperbranched polymers such as modifiable surface functionality, available internal cavities, uniform film and good solubility make them attractive for biological, chemical and medical field²⁸. In morphology aspect, the microstructure of films, which determined the quenching efficiency, response time *etc* has an important effect on the sensing performance. We find that using ZnO nanorods array as the substrate of the sensing film²⁹ can effectively increase the signal strength, reaction rate and sensitivity due to high area to volume ratio for efficient analyte permeability and catalytic ability of light oxidation³⁰. Herein, we systematically discussed that the effects of the configuration of polymer, chain end location and number of boron ester unit, as well as the polymers/ZnO nano rod array composite on the sensing performance of the peroxide vapor detection.

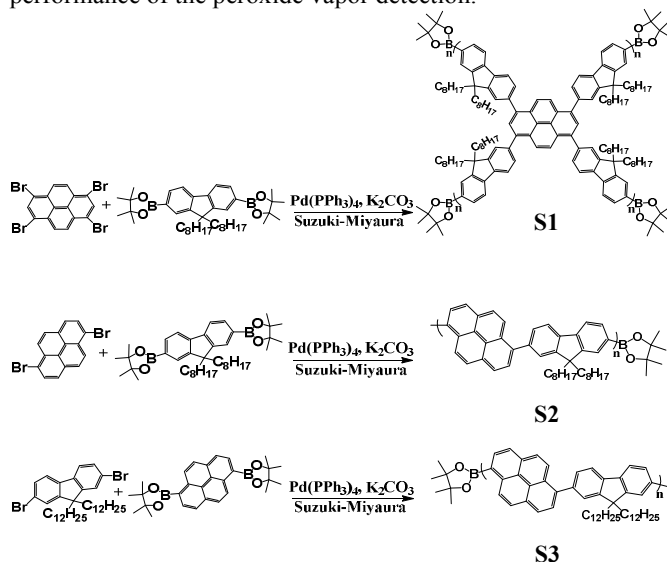


Figure 1. The polymerization of S1, S2 and S3.

2. Experimental Section

2.1 Instruments

The ¹H-NMR spectra were recorded on a Bruker DRX500 instrument, and tetramethylsilane (TMS) was used as an Internal standard. UV-Vis absorption and fluorescence analysis were obtained from a Jasco V-670 spectrophotometer and a Jasco FP 6500 spectrometer, respectively. High vacuum infrared spectra were performed on Bruker VERTEX 70v *via* surface reflection-absorption model. Cyclic voltammetry (CV) experiments were performed with a CH instruments electrochemical analyzer. The electrochemical behaviors of S1, S2 and S3 were investigated in a standard three electrode electrochemical cell (a glassy carbon working electrode, a platinum counter electrode and a silver chloride electrode as a reference electrode) with 0.1 M tetra-*n*-butylammonium hexafluorophosphate (Bu₄NPF₆) in acetonitrile solution, and the scanning rate was 100 mV/s under nitrogen atmosphere at room temperature.

2.2 Synthesis

All the chemicals and solvents were obtained from commercial sources and used as received. The synthetic procedures were

illustrated in **Figure 1**. All the polymers were synthesized *via* Suzuki-Miyaura cross-coupling reaction with yields of 34%, 41% and 48%, respectively. The raw materials, 1, 3, 6, 8-Tetrabromopyrene, 9, 9-dioctyl-2, 7-bis (boronic acid pinacol ester) fluorene, 1, 6-Dibromopyrene, 2, 7-dibromo-9, 9-didodecyl-fluorene and 2, 7- bis (4, 4, 5, 5-tetramethyl-1, 3, 2-dioxaborolan-2-yl) - pyrene were obtained from commercial resources.

2.2.1 Polymerization of S1

A mixture of 1, 3, 6, 8-Tetrabromopyrene (0.156 g, 0.301 mmol), 9, 9-dioctyl-2, 7-bis (boronic acid pinacol ester) fluorene (0.951 g, 1.480 mmol), Pd(PPh₃)₄ (98.6 mg, 0.085 mmol), K₂CO₃ (aq, 2 M/10 mL), dioxane (20 mL), ethanol (10 mL) and aliquat 336 (two drops) was charged under nitrogen and stirred for 24 h at 100 °C. After cooling to room temperature, the solution was washed with water/CH₂Cl₂ solution and dried with MgSO₄. The organic phase solution was evaporated under reduced pressure to get crude solid product. The crude polymer was then dissolved with least amount of toluene and precipitated in methanol for three times. The polymer was then further purified by a short silica column with THF as eluent and precipitated in MeOH again. The final product was dried to afford the polymer as a light green solid (234 mg, 34%). ¹H-NMR (500 MHz, CDCl₃, 25 °C, TMS): δ= 8.20 (s, 4H), 8.07 (s, 2H), 7.85 (d, 4H), 7.83 (d, 4H), 7.78 (t, 8H), 7.67(d, 8H), 2.04 (s, 20H), 1.26 (m, 30H), 1.12 (m, 90H), 0.83 (m, 50H). GPC (THF vs. PS): Mn= 2875, Mw= 3514, PDI=1.22.

2.2.2 Polymerization of S2

Following the same polymerization procedure as S1, with 1,6-Dibromopyrene (277.2 mg, 0.77 mmol), 9, 9-dioctyl-2, 7-bis (boronic acid pinacol ester) fluorene (0.73 g, 1.136 mmol), Pd(PPh₃)₄ (89 mg, 0.077 mmol), K₂CO₃ (aq, 2 M/10 mL), tetrahydrofuran (20 mL) and aliquat 336 (four drops). The final product was dried to afford S2 as a celadon solid (250 mg, 41%). ¹H-NMR (500 MHz, CDCl₃, 25 °C, TMS): δ= 8.34 (m, 3H), 8.15 (m, 3H), 8.09 (m, 1H), 7.83 (m, 2H), 7.73 (m, 2H), 7.65(m, 2H), 2.16 (s, 2H), 2.08 (s, 2H), 1.43 (s, 2H), 1.25 (m, 18H) 0.97 (m, 14H), 0.84 (m, 6H). GPC (THF vs. PS): Mn= 4819, Mw= 6981, PDI=1.45.

2.2.3 Polymerization of S3

Following the same polymerization procedure as S1, with 2, 7-dibromo-9, 9-didodecyl-fluorene (330 mg, 0.5 mmol), 2, 7-bis(4, 4, 5, 5-tetramethyl-1, 3, 2-dioxaborolan-2-yl)-1, 6-dihydropyrene (340 mg, 0.75 mmol), Pd(PPh₃)₄ (60 mg, 0.05 mmol), K₂CO₃ (aq, 2 M/15 mL), toluene (15 mL) and aliquat 336 (four drops). The final product was dried to afford the polymer as a light brown solid (170 mg, 48%). ¹H-NMR (500 MHz, CDCl₃, 25 °C, TMS): δ= 8.53 (m, 3H), 8.25 (m, 4H), 7.95 (m, 8H), 2.18 (m, 4H), 1.25 (s, 8H), 1.22 (s, 48H), 0.88 (m, 18H). GPC (THF vs. PS): Mn= 8278, Mw= 27905, PDI=3.371.

2.3 Vapor sensing experiment

The sensing films were prepared by dip-coating toluene solutions (10⁻⁴ M) of S1, S2 and S3 onto 10 × 20 mm quartz plate and vacuum-dried for half an hour before use. The fluorescence responses of films to peroxide were progressed by inserting the films into hermetically-sealed vials (3.8 mL) containing cotton and analyte at room temperature, which could prevent the direct contact between the probe and analyte as well as help to maintain a constant vapor pressure. The fluorescent

time-course responses were recorded as soon as the film was exposed to analyte vapor and ended at 300 s.

3. Result and discussion

3.1 Optical and electrochemical properties

Figure 2 shows the absorption and emission spectra of **S1**, **S2** and **S3** in films and in THF solution. Their photophysical results are summarized in **Table 1**. On the one hand, it can be found that the maximum absorption peak of linear polymers **S2** and **S3** in THF are 383 and 346 nm, respectively. Compared with that of **S2**, the maximum absorption peak of **S3** is blue-shifted by 37 nm and the similar result also appears in the film state. This proves that a different connection position of borate ester unit has a different effect on the spectral characteristics. On the other hand, the emission peak of hyperbranched polymer **S1** in THF is 465 nm, red-shifted by 28 nm compared to that of **S2**. The same result was also observed in film state (red-shifted by 20 nm). The borate ester number of **S1** in one molecule unit is more than that of **S2**, and there are different configurations in **S1** (hyperbranched polymer) and **S2** (linear polymer), which leads to more efficient conjugation in **S1**. It is easy to find that the number of borate esters on the chain end and configuration of polymer have different impact on the spectral property.

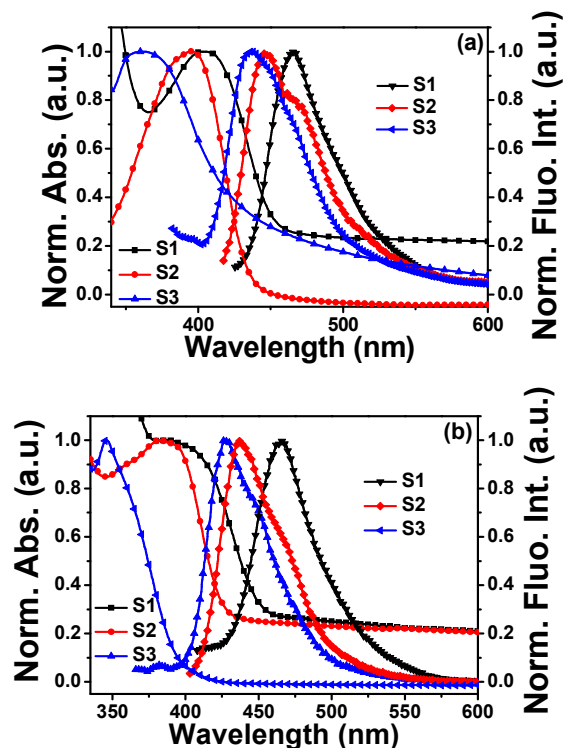


Figure 2. UV-Vis absorption and emission spectra of **S1**, **S2** and **S3** in films (a) and in THF solution (concentration, 10^{-6} M) (b).

The emission peak of **S2** and **S3** films are red-shifted by 9 and 10 nm from solution to film state respectively, while that of **S1** film is almost the same (a red shift of only 1 nm). The result illustrates the hyperbranched structure of **S1** has larger steric hindrance and it is beneficial for preventing the π - π stacking caused self-aggregation effect in solid state and hence improving the sensing performance. In addition, both **S1** and **S2** have very high fluorescent quantum yield (Φ) in their THF solution, which are nearly 1. It is also an important factor as sensing materials. Moreover, Stokes shifts of **S1** and **S3** are larger than that of **S2** in both solution state and solid state, which can avoid the self-absorption by the material and reduce the interference of the background to improve the sensitivity. Last but not the least, there are plenty of internal cavities³¹ and external boron ester groups in hyperbranched configuration of **S1** so that it makes important contributions to increasing permeability of analytes and response rate of the sensing process.

The energy level is related to the probe's reactivity to the oxidation reagents. The electrochemical results (**Table 1**) reveal that the HOMOs of **S1**, **S2** and **S3** are -5.49, -5.99 and -6.04 eV, respectively, suggesting a stepwise decreased HOMO from **S1** to **S3**. Their band gaps are 2.80, 3.21 and 3.25 eV and **S1** is the least one among them. These features mean that **S1** will be likely the most reactive polymer toward oxidation reaction. The hyperbranched molecular structure and more borate ester groups on the periphery structure of **S1** make it more efficient conjugation and more reactive than the linear polymers **S2** and **S3**. At the same time, narrow band gap means that **S1** needs an exciting light with longer wavelength. Thus, it can not only reduce the cost of the detector but also improve the light stability of the material. All these optical and electrochemical conditions above suggest the hyperbranched polymer **S1** is likely a promising candidate for fluorescent sensing application.

3.2 Detection of peroxide in the vapor phase

The sensing performances of the three polymers to peroxide vapor were monitored by fluorescent spectroscopy. The films were fabricated by dip-coating their toluene solution with a concentration of 10^{-4} g/mL onto quartz plate. The normalized peak emission intensity change in air or explosive vapour with time is shown in **Figure 3**. It exhibits that the quenching efficiency of three probes towards the saturated vapor of 30% H_2O_2 aqueous are 40% (**S1**), 24% (**S2**) and 23% (**S3**) respectively. As can be seen, the hyperbranched polymer **S1** shows a much better sensing performance than that of the linear polymer **S2** and **S3**.

Table 1. Optical and electrochemical properties of **S1**, **S2** and **S3**.

	Abs, λ_{max} (nm)		PL, λ_{max} (nm)		HOMO (eV)	LUMO (eV)	ΔE (eV)	Φ^a
	solution	film	solution	film				
S1	388	400	465	466	-5.49	-2.69	2.80	0.89
S2	383	396	437	446	-5.99	-2.78	3.21	1
S3	346	361	427	437	-6.04	-2.79	3.25	0.39

^a The fluorescence quantum yields of S1, S2 and S3 compounds in THF dilute solution were measured using a dilute solution of 9,10-diphenylanthracene ($\Phi \sim 1$) in THF solution as the standard.

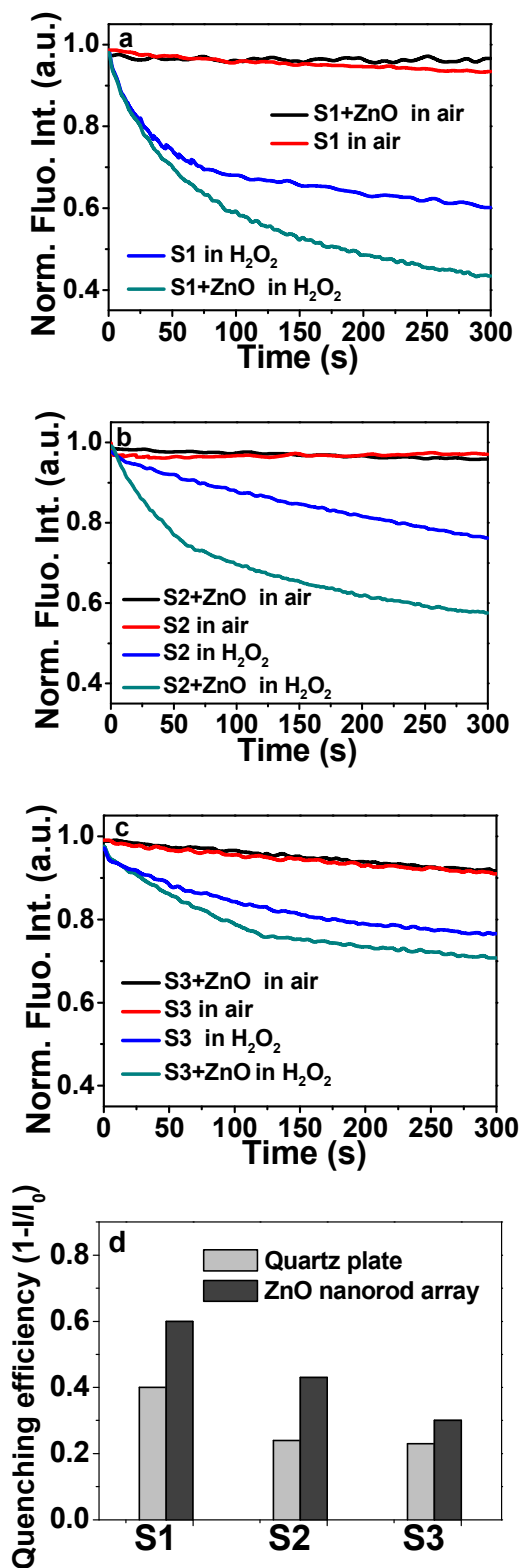


Figure 3. (a-c) Stability and sensing properties of S1-S3 films on different substrates exposed to air and H₂O₂ saturated vapor respectively within 300s. (a: S1; b: S2; c: S3); (d) Quenching efficiency of S1-S3 films on different substrates in H₂O₂ saturated vapor within 300s.

Since the sensing performance is also related to their film morphology. SEM was used for the morphology characterization. **Figure 4** shows that more uniform film is formed for hyperbranched polymer S1, while S2 and S3 suffered a heavy aggregation. SEM results suggest that the linear polymer structure with polar borate ester end groups will lead to serious aggregation, which not only prevents the penetration of H₂O₂ vapor but also reduces the specific surface area of films resulting in a lower sensitivity.

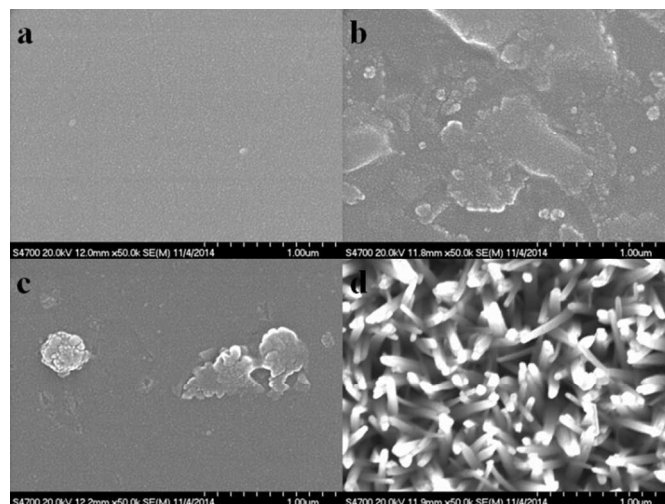


Figure 4. SEM images of S1-S3 films prepared with toluene solvents (all concentrations, 10⁻³ g/ml) and ZnO nanorod array as film substrate (a: S1; b: S2; c: S3; d: ZnO nanorod array).

The morphology of the substrate may also greatly influence the sensitivity, since a high specific surface area and surface activity of the films will contribute to the sensing performance. Our group has successfully developed ZnO nanorod arrays with different surface morphology and proved to improve the sensing efficiency by a catalytic functionality to accelerate the reaction rate and evanescent effect to increase the emission intensity²⁹. Therefore, we coated the fluorescent materials on the surface of ZnO nanorod arrays (Figure 4(d)) vertically arranged on quartz plate to make it a composite. **Figure 3 (a)** presents that the S1/ZnO nanorod arrays composite produces enhanced fluorescence quenching with a response rate of about 30% within 50 s and finally 60% within 300 s upon exposure to a vapor of 30% H₂O₂ aqueous, corresponding to a 20% increase relative to that on quartz plate. Under the same condition, the quenching efficiency of hyperbranched polymer S1 to H₂O₂ vapor is also much better than that of linear polymer S2 and S3 (43% and 30% quenching efficiency within 300 s, respectively). It demonstrates hyperbranched polymer S1 with more external boron ester end groups and internal cavities is conducive to peroxide vapor penetration and contributes to more effective detection.

In order to interpret the sensing mechanism, both fluorescence and high vacuum reflection-absorption infrared spectra (IRAS) were used for monitoring the changes of S1/ZnO nanorod array composite film before and after the H₂O₂ vapor exposure. Figure 5 (a) shows that emission changes of S1 by dissolving the composite film into THF after being exposed to H₂O₂ in a period of 20 minutes. The emission peak of S1 declines gradually with a slight red shift from 461 to 465 nm. Figure 5 (b) exhibits the IRAS changes that, after the exposure, the band at 1343 cm⁻¹ (B-O characteristic peak) disappears along with the appearance of new band at 3253 cm⁻¹ (O-H characteristic peak). It proves that the deboronation reaction occurred between external boron ester end groups of S1 and peroxide vapor leading to the fluorescence turn-off as shown as Figure 5 (c). In addition, the fluorescent conjugated structure of hyperbranched polymer S1 can amplify fluorescence signal due to its effective conjugation and multiple borate esters structure. On the other hand, ZnO nanorod arrays not only change the surface morphology of the film but also increase the reactivity to H₂O₂ vapor, which will accelerate the deboronation reaction of S1 under UV light³⁰.

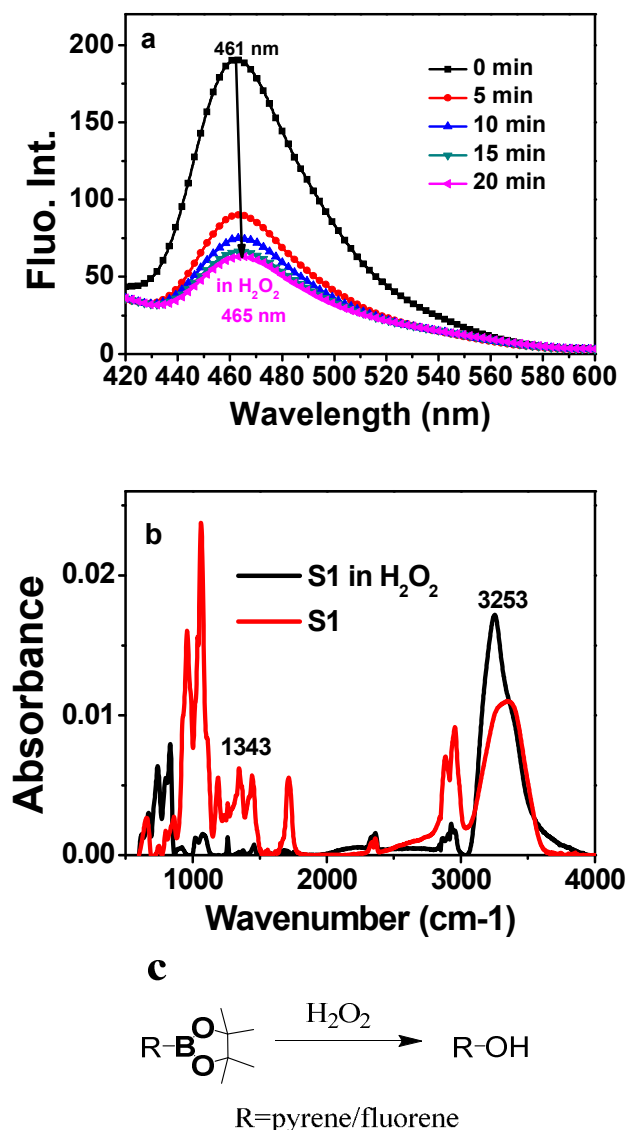


Figure 5. (a) Changes in the emission spectral pattern of S1 film on ZnO nanorod array during reaction with H₂O₂ saturated vapor followed by dissolving the film into THF solvent within the reaction of 20 minutes. (b) High vacuum infrared spectra of S1/ZnO nanorod array composite dissolved into THF solution before (red) and after exposure to hydrogen peroxide (black) vapor for 1h. (c) Deboronation reaction of boron ester group by H₂O₂.

The light stability will determine the lifetime of the sensing devices. The photo bleaching of S1 on quartz plate is measured to be ~7% in 300 s under air condition. However, the light bleaching of S1/ZnO nanorod arrays composite can be well controlled within 2% suggesting that ZnO nanorod arrays are also favorable for enhancing the stability of material. Nevertheless, compared with the good stability of S1 and S2, the photo bleaching rate of S3 film either on quartz plate or on ZnO nanorod arrays is not ideal (~9%). The results illustrate that the connection position of borate ester groups has obvious influence on light stability and the sensing performance of sensing films. A direct connecting borate ester to fluorene causes better light stability and sensing performance than that to pyrene. This is likely relevant to the increased intermolecular interaction among pyrene molecules due to the polar borate ester units. S3 film is very difficult to be used as efficient sensor due to worse photo stability which leads to a short lifetime and false alarm signals of the detection device.

The selectivity is another important issue for the sensing performance. Figure 6 shows fluorescence responses of S1/ZnO composite to different analytes saturated vapor. S1 film presents obvious fluorescent quenching response to H₂O₂ (~60%) and TATP (~30%). It is mentionable that compared with H₂O₂, TATP is hard to be detected with high sensitivity owing to the lower saturation vapor pressure (78 ppm). Hence S1 will be a promising fluorescent probe for TATP vapor detection. The other common used solvents vapor such as methylene chloride, acetone and ethyl alcohol show very low quenching efficiencies, which will not interfere with the sensing process. It is important to note that some solvents such as toluene can lead to enhanced fluorescence intensity due to swelling effect. But it will not produce interference to the peroxide detection based on fluorescence quenching process. In addition, the quenching efficiencies of S1 to some saturated vapor mixtures of different analytes after an exposure of 300 s are all less than 15% so that it will not interfere with the sensing process (As shown as Figure S4).

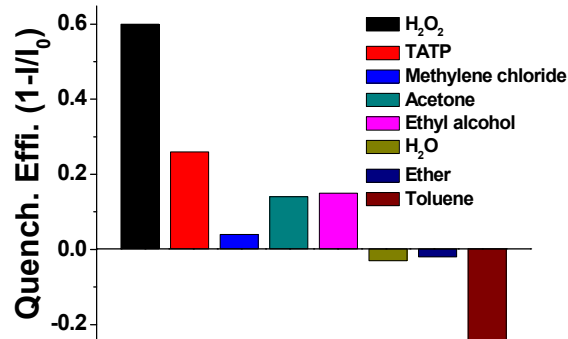


Figure 6. Fluorescence responses of S1 film on ZnO nanorod array to different compounds saturated vapor after an exposure of 300s.

In order to determine the detection limit of the S1/ZnO nanorod array composite film, diverse concentrations of H₂O₂ solution were prepared by diluting the 30 wt% H₂O₂ solution with deionized water to produce a corresponding equilibrium vapor pressure (1, 19, 38 and 225 ppm, corresponding to 90, 10, 5, and 1 times dilution of the commercial 30 wt% H₂O₂ solution) at room temperature (25 °C)³². The quenching efficiencies towards different concentration of H₂O₂ vapor are shown in **Figure 7 (a)**. Then the different quenching rates and corresponding equilibrium vapor pressures data were made a linear fitting, which is well-fitted to the Langmuir equation. As shown as **Figure 7 (b)**, the detection limit of H₂O₂ could be as low as 1.6 ppb if the triple multiple signal to noise ratio of the fluorescent detection device was considered as 0.01.

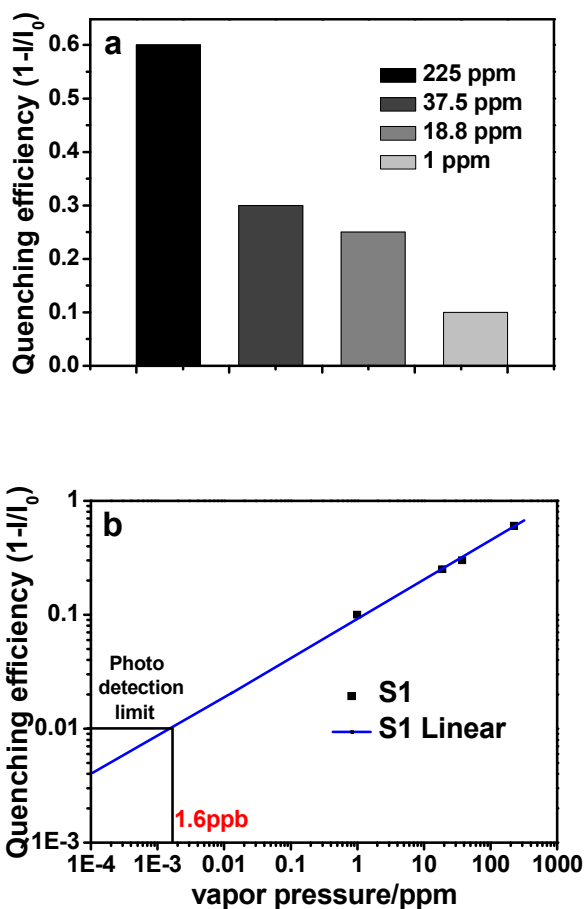


Figure 7. (a) Quenching efficiency of S1 film on ZnO nanorod array to different vapor pressure of H₂O₂ after an exposure of 300s. (b) Quenching efficiency of S1 film on ZnO nanorod array as a function of the vapor pressure of H₂O₂ fitted with Langmuir equation.

4. Conclusions

In summary, we reported a relatively simple, sensitive and selective borate ester endcapped pyrene-fluorene hyperbranched copolymer for fluorescent detection of peroxide explosive vapor. The sensing performance is based on a deboration reaction under peroxide and signal amplification effect of polymer resulting in fluorescence quenching, which is related to the molecular structure, substitution position on the aromatic ring and the numbers of the borate units. A composite

of the sensory polymer/ZnO nanorod array can improve the stability and sensibility of material because of the catalytic ability of light oxidation and surface morphology with high area to volume ratio for efficient analyte permeability. The results show that compared with two linear analogues S2 and S3, the hyperbranched polymer S1 demonstrates more sensitive response toward peroxide (~60% quenching and 30% for TATP within 300 s) due to larger steric hindrance, higher HOMO level, more internal cavities and external boron ester groups of hyperbranched structure. The detection limit to H₂O₂ vapor is estimated to be 1.6 ppb. This method provides a new way for trace and on-site chemical detection of peroxide-based explosives (PEs) for human health and public safety.

Acknowledgements

This work is supported by National Nature Sciences Foundation of China (No. 61325001, 21273267, 61321492, 51473182), the Shanghai Science and Technology Committee (No. 11JC1414700), and Shanghai Municipal Commission of Economy and Informatization. We would also like to express our thanks to Mr. Pengcheng Xu for IR measurement and helpful discussions.

Notes and references

^a State Key Lab of Transducer Technology, Shanghai Institute of Microsystem and Information Technology, Chinese Academy of Sciences, Changning Road 865, Shanghai 200050, China. E-mail: hqg@mail.sim.ac.cn, jgcheng@mail.sim.ac.cn

^b University of Chinese Academy of Sciences, Yuquan Road 19, Beijing 100039, China

† Electronic Supplementary Information (ESI) available: [Fourier transform infrared spectra of S3, S2, S1 and the contrast, The GPC and CV curves of S1-S3 polymer, The quenching efficiency (1-I/I₀) of S1 film on ZnO nanorod array to different vapor pressure of H₂O₂ after an exposure of 300s]. See DOI: 10.1039/b000000x/

- S. Meyer, *Secur. J.*, 2012, **25**, 309-325.
- J. Roach, P. Ekblom and R. Flynn, *Secur. J.*, 2005, **18**, 7-25.
- S. W. Thomas, G. D. Joly and T. M. Swager, *Chem. Rev.*, 2007, **107**, 1339-1386.
- M. E. Germain and M. J. Knapp, *Chem. Soc. Rev.*, 2009, **38**, 2543-2555.
- T. Naddo, Y. Che, W. Zhang, K. Balakrishnan, X. Yang, M. Yen, J. Zhao, J. S. Moore and L. Zang, *J. Am. Chem. Soc.*, 2007, **129**, 6978-6979.
- C. Zhang, Y. Che, X. Yang, B. R. Bunes and L. Zang, *Chem. Commun.*, 2010, **46**, 5560-5562.
- J. W. Grate, R. G. Ewing and D. A. Atkinson, *Trends Anal. Chem.*, 2012, **41**, 1-14.
- C. Chen, R. Y. Wang, L. Q. Guo, N. Y. Fu, H. J. Dong and Y. F. Yuan, *Org. Lett.*, 2011, **13**, 1162-1165.
- Y. Liu, C. Deng, L. Tang, A. Qin, R. Hu, J. Z. Sun and B. Z. Tang, *J. Am. Chem. Soc.*, 2011, **133**, 660-663.
- S. Shanmugaraju, S. A. Joshia and P. S. Mukherjee, *J. Mater. Chem.*, 2011, **21**, 9130-9138.
- H. N. Kim, W. X. Ren, J. S. Kim and J. Yoon, *Chem. Soc. Rev.*, 2012, **41**, 3210-3244.
- Z. Huang, J. Du, J. Zhang, X. Q. Yu, and L. Pu, *Chem. Commun.*, 2012, **48**, 3412-3414.
- C. Rena, J. S. Leea and T. E. Glassa, *Supramol. Chem.*, 2014, **26**, 607-611.
- R. Schulte-Ladbeck, M. Vogel and U. Karst, *Anal. Bioanal. Chem.*, 2006, **386**, 559-565.

- 15 G. M. Whit, *J. Forensic. Sci.*, 1992, **37**, 652–656.
- 16 G. J. McKay, *Kayaku Gakkaishi*, 2002, **63**, 323–329.
- 17 P. Wilson, B. Prince and M. McEwan, *Anal. Chem.*, 2006, **78**, 575–579.
- 18 F. Dubnikova, R. Kosloff, J. Almog, Y. Zeiri, R. Boese, H. Itzhaky, A. Alt and E. Keinan, *J. Am. Chem. Soc.*, 2005, **127**, 1146–1159.
- 19 M. E. Germain, M. J. Knapp, *Inorg. Chem.*, 2008, **47**, 9748–9750.
- 20 F. Hu, Y. Y. Huang, G. X. Zhang, R. Zhao, D. Q. Zhang, *Tetrahedron Lett*, 2014, **55**, 1471–1474.
- 21 Y. Ling, N. Zhang, F. Qu, T. Wen, Z. F. Gao, N. B. Li, H. Q. Luo, *Spectrochim. Acta, Part A*, 2014, **118**, 315–320.
- 22 M. W. Todd, R. A. Provencal, T. G. Owano, B. A. Paldus, A. Kachanov, K. L. Vodopyanov, M. Hunter, S. L. Coy, J. I. Steinfeld and J. T. Arnold, *Appl. Phys. B*, 2002, **75**, 367–376.
- 23 D. Muller, A. Levy, R. Shelef, S. Abramovich-Bar, D. Sonenfeld and J. Tamiri, *Forensic. Sci.*, 2004, **49**, 935–938.
- 24 P. F. Wilson, B. J. Prince and M. J. McEwan, *Anal. Chem.*, 2006, **78**, 575–579.
- 25 G. A. Buttigieg, A. K. Knight, S. Denson, C. Pommier and M. B. Denton, *Forensic. Sci. Int.*, 2003, **135**, 53–59.
- 26 M. Xu, J. M. Han, Y. Q. Zhang, X. M. Yang and L. Zang, *Chem. Commun.*, 2013, **49**, 11779–11781.
- 27 M. Xu, J. M. Han, C. Wang, X. M. Yang, J. Pei and L. Zang, *ACS Appl. Mater. Interfaces*, 2014, **6**, 8708–8714.
- 28 A. K. Patri, I. J. Majoros and J. R. Baker, *Curr. Opin. Chem. Biol.*, 2002, **6**, 466–471.
- 29 D. F. Zhu, Q. G. He, Q. Chen, Y. Y. Fu, C. He, L. Q. Shi, X. Meng, C. M. Deng, H. M. Cao and J. G. Cheng, *ACS Nano*, 2011, **5**, 4293–4299.
- 30 C. He, D. F. Zhu, Q. G. He, L. Q. Shi, Y. Y. Fu, D. Wen, H. M. Cao and J. G. Cheng, *Chem. Commun.*, 2012, **48**, 5739–5741.
- 31 Q. G. He, H. M. Huang, F. L. Bai and Y. Cao, *Macromol. Rapid Commun.*, 2006, **27**, 302–305.
- 32 S. L. Manatt, M. R. R. Manatt, *Chem.-Eur. J.*, 2004, **10**, 6540–6557.